


## Why has Precipitation Increased in the Last 120 Years in Norway?

K. Konstali<sup>1,2</sup>  and A. Sorteberg<sup>1,2</sup> 

<sup>1</sup>Geophysical Institute, University of Bergen, Bergen, Norway, <sup>2</sup>Bjerknes Center for Climate Research, Bergen, Norway

### Key Points:

- Precipitation has increased by more than 19% over the last 120 years in Norway
- We decompose changes in precipitation into changes in thermodynamics and dynamics
- Vertical velocity is the dominant driver for interannual variability in precipitation in Norway

### Supporting Information:

Supporting Information may be found in the online version of this article.

### Correspondence to:

K. Konstali,  
kjersti.konstali@uib.no

### Citation:

Konstali, K., & Sorteberg, A. (2022). Why has precipitation increased in the last 120 years in Norway? *Journal of Geophysical Research: Atmospheres*, 127, e2021JD036234. <https://doi.org/10.1029/2021JD036234>

Received 19 NOV 2021  
Accepted 22 JUN 2022

**Abstract** We use a data set with daily precipitation observations from 55 homogeneity-tested stations in Norway from 1900 to 2019 available from MET-Norway. These observations show that precipitation in Norway has increased by 19% since 1900. Notably, over half of the overall increase occurred within the decade of 1980–1990 and is happening across all precipitation rates. To examine possible mechanisms behind the precipitation increase, we use a diagnostic model to separate the effects of changes in vertical velocity, temperature and relative humidity. We use daily vertical velocity, near-surface temperature and relative humidity from two reanalysis products, ERA-20C and 20th Century Reanalysis. The model-based precipitation correlates significantly with the observed precipitation on an annual timescale ( $r > 0.9$ ), as well as captures the trend in all reanalysis products. The diagnostic model indicates that the variability in vertical velocity chiefly determines the interannual variability and long-term trend. The trend in vertical velocities contributes to more than 80% of the total modeled trend in precipitation between 1900 and 2019. However, over the last two decades (1995–2015), changes in temperature and relative humidity are the main contributors to the modeled trend in precipitation.

## 1. Introduction

Norway is located at the end of the North-Atlantic storm track and is thus warmer and wetter than the average climate at the same latitude, as cyclones transport heat and moisture poleward. Between 1900 and 2014, precipitation in Norway has increased by more than 18% (Hanssen-Bauer et al., 2017). Furthermore, Northern Europe is one of the few regions globally where there is high confidence that human influence has contributed to the observed changes in extreme precipitation (Seneviratne et al., 2021). Precipitation is expected to increase in Europe with continued warming (Seneviratne et al., 2021), and the relative change in extreme precipitation is expected to increase faster than the mean (Kharin et al., 2007; Myhre et al., 2019; Sillmann et al., 2013). Knowledge is currently lacking on how precipitation extremes have changed in Norway, on the changes in precipitation characteristics, and a discussion of possible mechanisms behind the precipitation increase. To close this gap, we analyze an extensive station network with data from 1900 and provide an updated and consistent view of mean and extreme precipitation changes. Furthermore, we examine possible mechanisms behind the precipitation variability and link it to thermodynamic and dynamic changes using a diagnostic model to decompose the observed changes into contributions from vertical velocity, temperature, and relative humidity.

Precipitation is expected to increase in a warmer climate because higher temperatures are related to increased precipitation through moisture availability. If the relative humidity is constant, the atmosphere's moisture content scales directly with the saturation vapor pressure, which increases with rising temperatures (Clausius, 1850). At our current temperature, this means an increase in atmospheric water vapor content of approximately 7% K<sup>-1</sup> (Trenberth et al., 2003). The thermodynamic contribution to extreme precipitation change is well understood and positive everywhere (Pfahl et al., 2017), and it can also be interpreted as the maximum amount the mean precipitation can increase at a regional level if the relative humidity and upward vertical velocity are constant. However, this effect is insufficient to explain the observed precipitation increase in Norway; while the temperature in Norway has increased by 1 K, precipitation increased by 18% (Hanssen-Bauer et al., 2017).

Thus, we must consider the dynamic changes in addition to the thermodynamic changes. Atmospheric circulation and associated vertical velocities comprise the dynamic component. This component is one of the major sources of uncertainty in climate models (Shepherd, 2014), and even the sign of the dynamic contribution to precipitation change differs between climate models in the same region (Pfahl et al., 2017; Seneviratne et al., 2021). The historical simulations of both CMIP6 and CMIP3 models produced considerably smaller trends in precipitation

© 2022. The Authors.

This is an open access article under the terms of the [Creative Commons Attribution License](https://creativecommons.org/licenses/by/4.0/), which permits use, distribution and reproduction in any medium, provided the original work is properly cited.

in Northern Europe than observed in the last century (van Haren et al., 2013; Vicente-Serrano et al., 2021). However, some of the CMIP6 models are able to capture the observed trend in the second half of the century (Vicente-Serrano et al., 2021). van Haren et al. (2013) linked the trend bias in CMIP3 to the circulation and sea surface temperature trend biases in the models' boundary conditions. As synoptic scale features, such as atmospheric rivers and extratropical cyclones (ETCs), are responsible for most extreme precipitation events in coastal Norway (Azad & Sorteberg, 2017; Benedict et al., 2019; Heikkilä & Sorteberg, 2012; Michel et al., 2021), dynamic changes have likely played a substantial role in changing the precipitation in the past.

Although thermodynamics' and dynamics' contributions to extreme precipitation changes are widely discussed, no studies have, to our knowledge, quantified the thermodynamic and the dynamic contributions to the observed mean precipitation increase over longer timescales using a physical diagnostic. Previous studies have quantified the thermodynamic and dynamic contributions to modeled extreme precipitation changes in the future (Pfahl et al., 2017; Tandon et al., 2018), changes in extreme precipitation over India between 1979 and 2019 (Ali & Mishra, 2018), and record-events of short timescales in the past (Oueslati et al., 2019). We adopt a similar framework to decompose the changes in mean precipitation into changes in thermodynamics and dynamics. We use a simplified model of precipitation that assumes pseudoadiabatic ascent and estimate the precipitation in Norway between 1900 and 2019 based on temperature, vertical velocity, and relative humidity. The method then allows us to decompose changes in precipitation into contributions from these three variables.

Although changes in precipitation in Norway have previously been investigated (e.g., Hanssen-Bauer, 2005; Hanssen-Bauer et al., 2017; Hanssen-Bauer & Førland, 1998; Hanssen-Bauer & Førland, 2000), there is currently no peer-reviewed literature on the topic. The most updated view on the trends used a monthly gridded data set (Hanssen-Bauer et al., 2017), and the interpolation uncertainties associated with such gridded precipitation datasets can be much larger than the uncertainties associated with measuring precipitation itself (Haylock et al., 2008). We avoid the interpolation uncertainties using the observations directly, although there may be issues of homogeneity in long precipitation time series (Hanssen-Bauer & Førland, 1994). In addition, none of the studies have considered changes in extreme precipitation in Norway since 1900. We aim to complement the existing literature on seasonal and annual mean changes by providing an updated view of the annual mean to daily extreme precipitation trends using daily observations over the last 120 years.

## 2. Data and Methods

### 2.1. Observations and Quality Control

We use observations of daily accumulated precipitation from The Norwegian Meteorological Institute. The data set is quality-controlled and has more than 200 stations all over Norway.

To select appropriate stations for our study, we check for sufficient data coverage in addition to homogeneity. For the data coverage, we require that the stations have less than 25% of the data missing between 1961 and 1990. Because some stations have changed location over the past 120 years, we merge data from stations closer than 4 km if the altitude difference is less than 100 m to get a longer continuous time series from the stations. We correct the shortest time series by multiplying it with the systematic bias, defined as the ratio of the longest to the shortest time series, if at least a 2 year data overlap exists. The results did not change much depending on a 2 or 4 km radius, but for an 8 km radius, the bias between the stations became substantially larger. The strict 100 m altitude difference was important to avoid merging a valley station with a mountain station. Then, to assure that a change of location, measuring technique, a merging of a station, or similar, have not artificially induced a trend in the time series, we check for breakpoints with a homogeneity test. The homogeneity test is a penalized maximum  $F$ -test (RHv4 Wang, 2008a; 2008b). If a breakpoint is detected within the time series at a 5% significance level, we remove the station from the record. Lastly, we visually inspect the time series and the remaining non-significant breakpoints. If a breakpoint is detected close to a station merging, or if the time series differ substantially from neighboring stations, we also remove these stations. The station metadata is available in Table S2 of Supporting Information S1.

Due to a shift in the number of stations in the late 1950s, we focus on two different periods: 1900–2019 and 1960–2019. In the time series starting in 1900, 69 stations meet the data coverage criteria. However, 14 of these did not pass the quality control, leaving 55 stations, of which 15 are merged with a neighboring station. Nearly all the stations are located in Southern Norway (Figure 1), while the two northernmost regions in Norway only

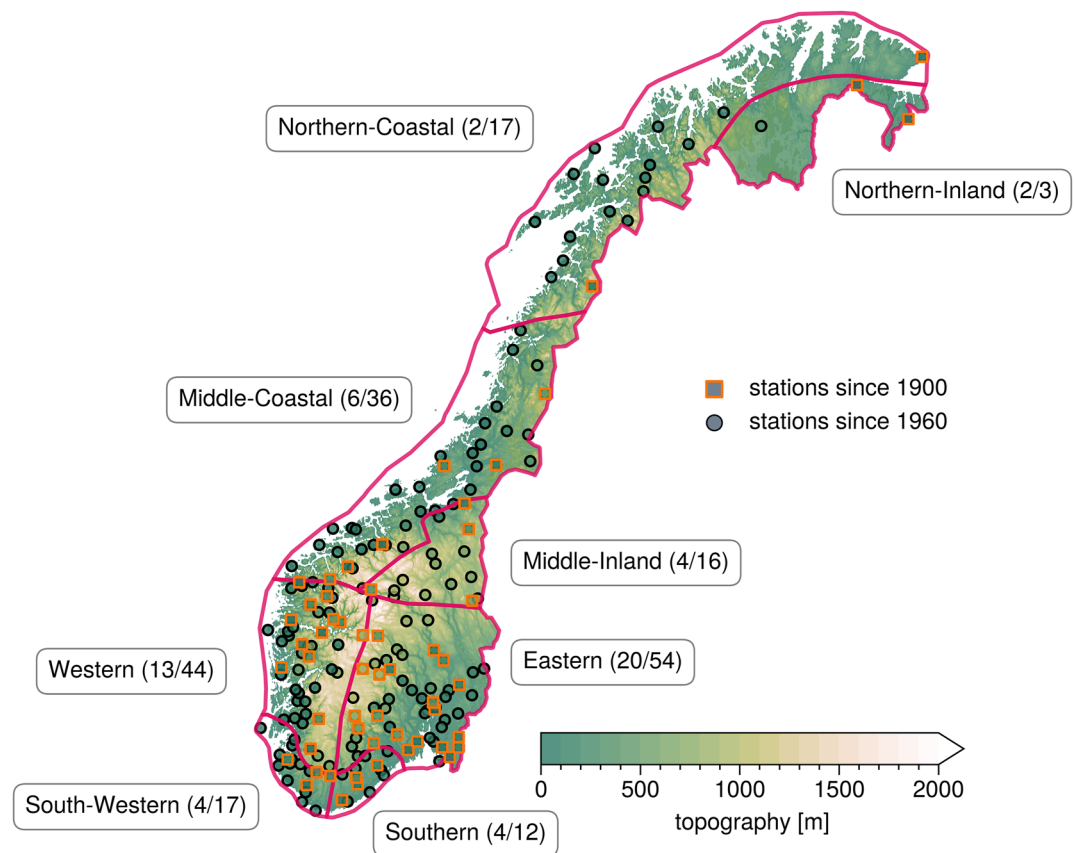


**Figure 1.** Map of Norway showing precipitation stations and the regions used in this study. Circles mark stations in the short time series and squares stations in the long time series. Colors indicate elevation. The numbers shown after the region names represent the number of stations available in the region from 1900 to 1960.

have two stations each. In the time series starting in 1960, 229 stations meet the data coverage criteria. Of these, 199 passed the quality control, and 64 stations were merged with a neighboring station. Despite the increase in the number of stations, most of them are still located in Southern Norway and at low elevations. We will refer to the aforementioned time-series of precipitation as OP1900 and OP1960, respectively.

We use the same precipitation regions as Michel et al. (2021), as shown in Figure 1. We refer to South-Western, Western, Middle-Coastal, Northern-Coastal, and Southern as coastal regions, and Middle-Inland, Northern-Inland and Eastern as inland, based on their seasonality characteristics of precipitation.

To calculate mean statistics for Norway, we weigh all regions equally regardless of area. This averaging method gives a bias toward Southern-Norway, where the regions are more numerous and smaller than the regions in Northern-Norway. However, the relative trend calculated for Norway of annual accumulated precipitation is almost insensitive to the choice of averaging methods (weighing all stations equally, weighing all regions equally, and weighing regions by area), differing only by 0.6%. We ignore the missing data and use only the existing values when we calculate the means for the individual stations. If the number of missing days exceeds 10% in a month, the monthly value for the station is assigned as missing.

## 2.2. Reanalyses

We use two reanalyzes products that provide global atmospheric data since 1900; European Centre for Medium-Range Weather Forecasts' (ECMWF) twentieth-century reanalysis, ERA-20C (Poli et al., 2016) and National Oceanic and Atmospheric Administration's (NOAA) Twentieth century Reanalysis version 3, 20CRv3 (Slivinski et al., 2019). Both are available on a  $1^\circ$  latitude  $\times$   $1^\circ$  longitude grid and at a 3 hourly temporal resolution. ERA-20 C has 91 vertical levels between the surface and 0.01 hPa, while 20CRv3 has 28 vertical levels from

the surface to 1 hPa. They both assimilate surface pressure, but ERA-20C assimilates marine winds in addition. For comparison and reference, we use ERA5 from ECWMF (Hersbach et al., 2020). ERA5 is available from 1979 to the present on a 30 km grid and has 137 levels in the vertical and an hourly temporal resolution.

We select 2 m temperature, dew point temperature or relative humidity, depending on availability, and vertical velocity in pressure coordinates from all available levels between 1,000 and 200 hPa at 12:00 UTC. We use the reanalyses at 12:00 UTC because there are more observations assimilated at this time step, particularly in the early part of the century (Cram et al., 2015).

### 2.3. Trend Analysis

We use the non-parametric Mann-Kendall test (Mann, 1945) to detect statistically significant trends in the time series. Because the test does not assume a distribution of the data, it is commonly used to detect trends in both mean and extreme precipitation (e.g., Alexander et al., 2006; Westra et al., 2013; Wu et al., 2016). If a trend is present in the time series, we use Sen's slope estimator (Sen, 1968) to calculate the magnitude of the trend. Note that “significant” refers to statistically significant at the 95% confidence level throughout the paper unless otherwise stated.

#### 2.3.1. Trend Analysis for Extreme Events

To determine the trend of different quantiles, we performed quantile regression on daily precipitation for each station following the method from Koenker and Hallock (2001). The advantage of using quantile regression compared to standard linear regression is that the quantile regression can estimate changes in all parts of the distribution rather than just the mean. While standard linear regression entails minimizing the sum of squared errors, quantile regression involves minimizing a weighted average of the absolute errors (Tareghian & Rasmussen, 2013). Several studies have used quantile regression to look at changes in extreme precipitation (e.g., Bohlinger & Sorteberg, 2018; Fan & Chen, 2016).

Rarer events, such as annual maxima, follow a Generalized-Extreme-Value (GEV) distribution and can thus be described with three parameters: location ( $\mu$ ), scale ( $\sigma$ ), and shape ( $\xi$ ). To determine whether trends are present in the annual maxima precipitation, we introduce time as a covariate to the location parameter,  $\mu = \mu_0 + \mu_1 t$ , where  $t$  is time. If the distribution with a varying location parameter is a better fit than a stationary location parameter according to a maximum-likelihood test with a 95% confidence level, we say that there is a significant trend in the annual maximum. Knowing the change in the location parameter allows us to calculate changes in both magnitude and return period for rare events, for example, 100 year events. We only used the stations available since 1900 to minimize the uncertainty in the calculated return values because the GEV distribution is highly sensitive to the record length (Hu et al., 2020). We use the extRemes software package, written in the statistical software language R (Gilleland & Katz, 2016), for extreme value analysis.

### 2.4. Diagnostic Model: Estimating Precipitation Based on Pseudoadiabatic Ascent

To relate trends in the observed precipitation to dynamically or thermodynamically induced changes, we use a diagnostic model based on moist pseudoadiabatic ascent. A similar formulation has been used by Sinclair (1994), Collier (1975), and Kunz and Kottmeier (2006) to model orographic precipitation. However, instead of using orographically induced velocity, we use the vertical velocity from reanalysis. We assume that all condensate precipitates out immediately and that no precipitation evaporates on the way down. Integrating the total condensate from the lifting condensation level to the top of the troposphere then yields the precipitation generated by the moist-pseudoadiabatic ascent, PAP, as formulated in Haltiner and Williams (1980, pp. 309–310):

$$PAP = \frac{\lambda_{RH}}{g} \int_{p_{LCL}}^{p_{top}} \delta_m \frac{q_s T}{R_p} \left( \frac{L_v R - c_p R_v T}{c_p R_v T^2 + q_s L_v^2} \right) \omega(p) dp . \quad (1)$$

In Equation 1,  $p_{LCL}$  and  $p_{top}$  are the pressure of the cloud base and 200 hPa, respectively.  $q_s$  is the saturation mixing ratio,  $\omega$  is the vertical velocity in pressure coordinates, which is a function of pressure ( $p$ ),  $T$  is temperature,  $R$  and  $R_v$  are the ideal gas constants for dry air and moist air, respectively, and  $L_v$  is the latent heat of vapourization.  $\delta_m$  is the Heaviside function which is 1 if the vertical velocity is upward and 0 otherwise and is evaluated at all levels. To avoid precipitation in unsaturated conditions but account for that part of the grid cell may be

saturated even if the average RH is below saturation, we introduce the RH-threshold parameter,  $\lambda_{RH}$ .  $\lambda_{RH}$  is 1 if  $RH > RH_c$  and 0 otherwise.  $RH_c$  is a critical relative humidity, set to 0.75 in every grid point, which according to Quaas (2012) is representative of pressure levels below 900 hPa over Europe as well as close to the mean global value at 1,000 hPa. For simplicity, we set the cloud base as the lifting condensation level, where air reaches saturation with a dry-adiabatic ascent from 1,000 hPa, estimated from the 2 m temperature and the 2 m relative humidity. Although keeping the sea level pressure constant is a simplification, we find the effect negligible as the results differ with  $<0.5\%$ . Within the cloud, we assume the air is saturated and that the temperature follows the moist-adiabatic lapse rate.

Equation 1 shows that precipitation depends on the upward vertical velocity inside the cloud and indirectly on the 2 m temperature and 2 m relative humidity, which affect the level of condensation, and thus the temperature within the cloud. We integrate all the levels with upward vertical velocity from the level of condensation to 200 hPa, where 200 hPa approximates the top of the troposphere.

#### 2.4.1. Separating the Effects of Changes in Vertical Velocity, Temperature, and Relative Humidity

To separate the contribution from changes in vertical velocity, temperature, and relative humidity to the long-term trend in precipitation, we decompose Equation 1. First, we construct a seasonal mean based on data from each day from all the years for the three variables at all pressure levels in a grid cell. Thereafter, we smooth the mean using a running 25 day average. The seasonal cycle of the vertical velocity is constructed from days with upward motion only at each pressure level. We then allow one term to vary on a daily timescale while keeping the seasonal cycle of the two other terms constant;

$$PAP \approx P_\lambda + P_{T^*} + P_{\omega^*} \quad (2)$$

$$= \lambda_{RH} \int_{p_{LCL}}^{p_{top}} [T^*] [\omega^*(p)] dp + [\lambda_{RH}] \int_{p_{LCL}}^{p_{top}} T^* [\omega^*(p)] dp + [\lambda_{RH}] \int_{p_{LCL}}^{p_{top}} [T^*] \omega^*(p) dp$$

where  $T^*$  is  $\frac{q_s T}{R_p} \left( \frac{L_v R - c_p R_v T}{c_p R_v T^2 + q_s L_v^2} \right)$ ,  $\omega^*$  is  $\delta_m(p)\omega(p)$ , and the square brackets denote the smoothed average seasonal cycle.  $P_\lambda$ ,  $P_{T^*}$ , and  $P_{\omega^*}$  thus represent the precipitation contribution from relative humidity, temperature, and vertical velocity, respectively. Despite the terms not being independent, their sum deviates little from that of the full equation with an average absolute error of 2.9%, 3.6%, and 3.1% in 20CRv3, ERA-20C, and ERA5, respectively, on an annual timescale. The small absolute errors indicate that the separation method is adequate and that the contributions from the interactive terms are small.

### 3. Observed Climatology and Trends

#### 3.1. Is the Station Network in the Long Time Series Representative?

As the station coverage increased substantially from 1900 to 1960 (55 stations to 199 stations), we check whether OP1900 represents precipitation on both a regional and national level compared to OP1960 (see Figure 1 for an overview of the spatial distribution of the stations). The national annual mean precipitation from OP1900 correlates near-perfectly to OP1960 ( $r = 0.99$ ). Furthermore, a linear regression of the monthly average precipitation from OP1900 to OP1960 reveals a mean slope of 0.98x, where x is the monthly average precipitation. Thus, OP1900 overestimates the monthly average precipitation by 2% compared to OP1960. However, OP1900 and OP1960 show a similar mean (difference  $<2.5\%$ ) and trend (difference  $<1\%$ ).

The high correlations between OP1900 and OP1960 can be explained by the high correlation between the stations in the coastal regions. For example, a station in Western correlates better to a station in Northern-Coastal more than 1,000 km away ( $r = 0.4$ ) than to a closer station in Eastern, only 250 km away ( $r = 0.1$ ).

With the number of stations and the correlation distances in mind, we do not have sufficient station coverage to calculate representative trends for Northern-Inland or Northern-Coastal. Northern-Inland has only two stations in OP1900 available, and they correlate poorly to each other because the correlation drops rapidly with distance ( $r = 0.2$ , mean distance = 100 km) and to stations in other regions ( $r < 0.2$ ). The station coverage in Northern-Coastal is also poor, with only two stations in OP1900. Although these stations are better correlated than in Northern-Inland ( $r = 0.4$ , mean distance = 250 km) and show a quite high correlation to Middle-Coastal ( $r = 0.4$ , mean distance = 650 km), it is impossible to determine whether they are representative of the region.

However, we will present the climatology for both regions based on OP1960, when the station coverage in Northern-Coastal improves substantially (from 2 to 17 stations).

The high correlation between the stations within regions and the linear regression slope parameter (close to 1) gives us confidence that we can use OP1900 to analyze changes in the mean and extreme precipitation of most regions and Norway as a whole between 1900 and 2019.

### 3.2. Observed Precipitation Climatology

We calculate the climatology for 1960–2019 to include as many stations as possible. Norway has a clear separation between the coastal and inland climates. In the coastal regions, humid air masses from the west meet the steep orography along the coastline and form orographically enhanced precipitation, which maximizes at the first orographic barrier before it decreases (Figure 2). Both the frequency of precipitation and the intensity are highest in Western and South-Western in all seasons (Figures 2b and 2c). It rains more than 45% of the days with an average of more than 10 mm/day (see table 1 for an overview). In contrast, Northern-Inland and Middle-Inland are the driest regions, reflected in both low mean wet day intensity (<6 mm/day) and wet day frequency (<33%).

The seasonal timing of precipitation is also different between the inland and coastal regions (Figure 2a). While most precipitation in the coastal region falls during September–November (SON), June–August (JJA) is the wettest season in the inland regions. March–May (MAM) is the driest season in coastal regions, whereas December–February (DJF) is the driest season in inland regions. Although JJA contributes relatively more to annual precipitation in the inland regions, the coastal regions are wetter in all seasons.

The distribution of the extreme precipitation (99th percentile) largely follows that of the observed climatology (Figure 2d). The 99th percentile is highest in Western Norway, and extreme precipitation events mainly occur in SON and DJF. Most extreme precipitation events occur in JJA and SON in the inland regions, and the 99th percentile is lower than in the coastal regions. However, the contribution from extreme precipitation to the annual total precipitation is higher in inland regions (15%–17%) than in coastal regions (12%–14%), and the proportion is increasing northwards (not shown).

The different seasonal cycles of precipitation and the differences in the rate at which correlation decrease with distance indicate different precipitation-generating mechanisms between the regions. That precipitation in coastal regions affects larger areas than in inland regions is consistent with precipitation events in coastal regions being of more synoptic-scale nature and directly associated with ETCs and westerly flow. This is consistent with Michel et al. (2021), who found that 82% of precipitation extremes in Western were associated with atmospheric rivers, which are linked to ETCs (e.g., Ralph et al., 2004). In contrast, <50% of extreme events in inland regions occurred with atmospheric rivers. This suggests that local convection and fewer or weaker ETCs dominate inland regions.

### 3.3. Trends and Changes in Time

The annual mean precipitation in Norway has increased by 19% between 1900 and 2019 (Figure 3a). The slightly larger value compared to Hanssen-Bauer et al. (2017) can be partly attributed to the inclusions of the years 2017–2019. It is also possible that the discrepancies come from different datasets used, as we use the station observations directly while Hanssen-Bauer et al. (2017) use a monthly gridded data set. Gridded datasets and observations have been shown to give different trends (Hanssen-Bauer et al., 2006). Precipitation has increased significantly in Western, Eastern, Middle-Coastal, Middle-Inland, and South-Western (see table 1 for an overview of all trends in all regions). Middle-Coastal has the largest relative increase (30.2%), but the region has no trend in the second half of the time series. In contrast, South-Western has the largest absolute increase (414 mm), with most of the increase after 1960 (402 mm). Lastly, five of the six regions with adequate data coverage exhibit a statistically significant trend at the 99% confidence level compared to the 4 of 13 regions in Hanssen-Bauer (2005).

Consistent with Hanssen-Bauer (2005), we find that precipitation in Norway since 1900 has increased in all seasons, but most in absolute magnitudes in SON (19.9%) and relative magnitudes in MAM (Figure 4, Figure S1 in Supporting Information S1). DJF is the only season without a significant trend in the long time series because of high interannual variability (however, the trend is still positive). Notably, almost half of the long-term increase occurred between 1980 and 1990 and was most prominent in DJF. Western and South-Western show the largest

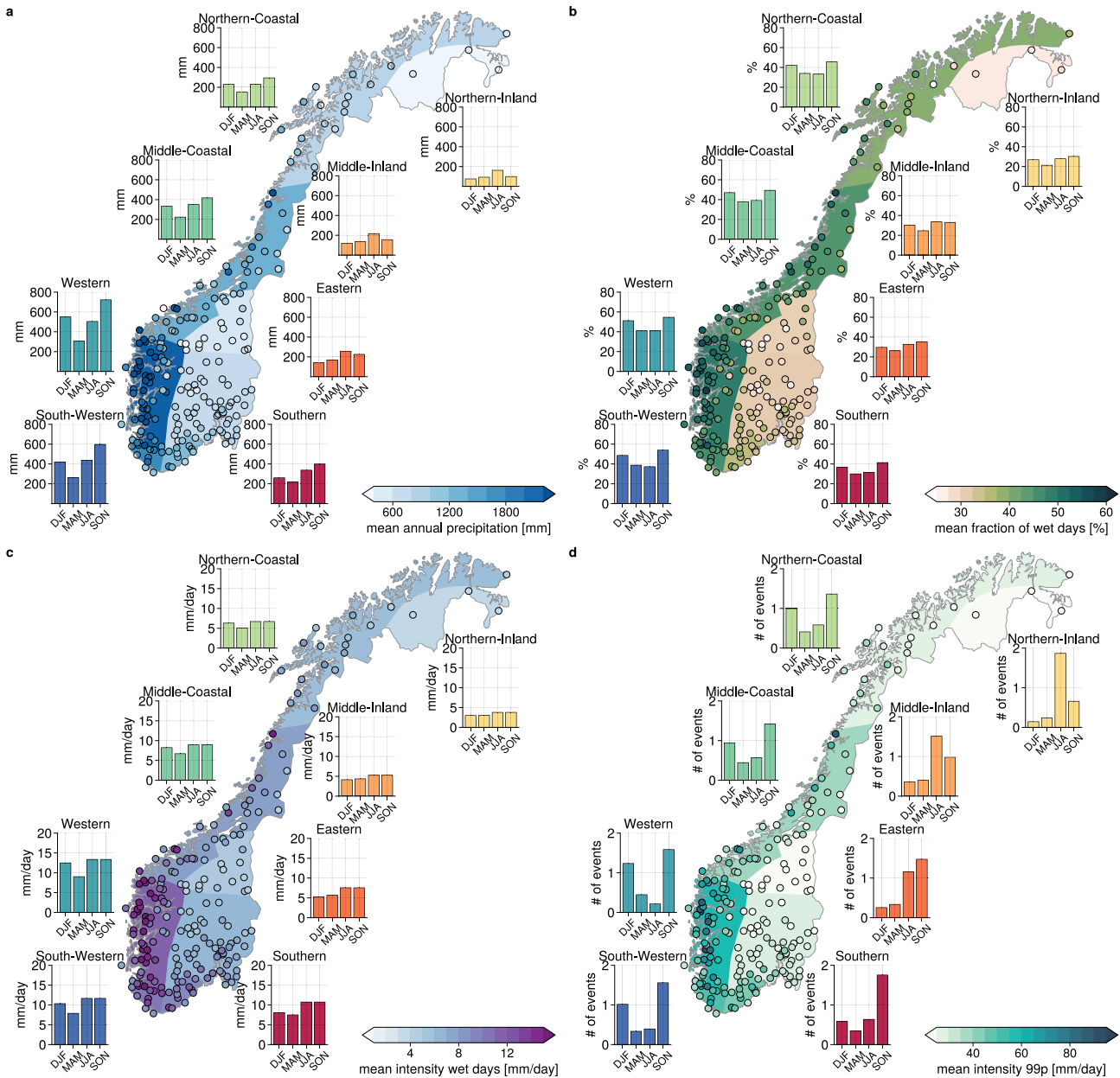


**Figure 2.** Spatial pattern of precipitation in Norway. Bars represent the seasonal average in the different regions. The map and individual stations are shaded according to (a) The annual mean precipitation in mm, (b) Wet day frequency, given in percent, and (c) mean intensity on the wet days in mm/day, (d) 99th percentile of daily precipitation amount (99p), while the bars represent the average number of events per year in the different seasons in the different regions.

increase, both in absolute and relative terms, but a signal is present in all regions (Figure 4 a, see Figure S1 in Supporting Information S1 for relative terms). This increase looks particularly dramatic because the years before 1980 were anomalously dry, while the years after were anomalously wet compared to the mean. The precipitation continued to increase after 1990, but at a lower rate and in all regions and seasons (Figures 4a–4d).

Both the frequency and intensity have contributed to the change in observed precipitation. In Norway, on average, between 1960 and 2019, the number of wet days increased by almost 10 days (6%, see Table 1), with an accompanying significant decrease in the annual longest dry spells (consecutive dry days, <1 mm/day). The trend in the absolute contribution of the precipitation rates to the annual total precipitation increase across all precipitation rates (Figure S2a in Supporting Information S1) indicates an overall increase in wet days, including an increase in

**Table 1**  
Trends in Mean Wet-Day Intensity Intensity, Annual Total, and the Number of Wet Days

			South-Western	Southern	Northern-Inland	Western	Eastern	Middle-Coastal	Middle-Inland	Northern-Coastal	Norway
Mean wet-day intensity	1900	mean [mm/day]	10.8	10.0	3.9	10.7	6.8	7.8	5.5	5.8	8.1
		rel	13.9 <sup>b</sup>	2.1	-	7.2 <sup>a</sup>	5.8 <sup>a</sup>	20.6 <sup>b</sup>	4.6	-	8.1 <sup>b</sup>
		abs	1.5 <sup>b</sup>	0.2	-	0.8 <sup>a</sup>	0.4 <sup>a</sup>	1.6 <sup>b</sup>	0.3	-	0.7 <sup>b</sup>
	1960	mean [mm/day]	10.1	9.2	4.0	11.4	6.7	7.9	5.1	6.1	8.2
		rel	12.5 <sup>b</sup>	5.2	1.4	11.1 <sup>a</sup>	7.3 <sup>a</sup>	9.2 <sup>a</sup>	7.9 <sup>b</sup>	9.3	9.4 <sup>b</sup>
		abs	1.3 <sup>b</sup>	0.5	0.1	1.3 <sup>a</sup>	0.5 <sup>a</sup>	0.7 <sup>a</sup>	0.4 <sup>b</sup>	0.6	0.8 <sup>b</sup>
Annual precipitation	1900	mean [mm/year]	1,772.7	1,362.1	381.1	1,850.5	803.0	1,230.8	686.9	785.4	1,189.1
		rel	23.4 <sup>b</sup>	9.0	-	17.3 <sup>b</sup>	18.3 <sup>b</sup>	30.2 <sup>b</sup>	22.4 <sup>b</sup>	-	20.0 <sup>b</sup>
		abs	414.5 <sup>b</sup>	123.0	-	319.9 <sup>b</sup>	147.1 <sup>b</sup>	371.9 <sup>b</sup>	154.0 <sup>b</sup>	-	236.6 <sup>b</sup>
	1960	mean [mm/year]	1,720.8	1,207.6	409.0	2,079.9	786.9	1,332.1	610.4	907.2	1,270.0
		rel	23.8 <sup>b</sup>	16.7	0.4	18.0	15.6 <sup>a</sup>	10.2	14.4 <sup>b</sup>	4.9	17.2 <sup>b</sup>
		abs	408.8 <sup>b</sup>	201.3	1.8	372.3	122.7 <sup>a</sup>	135.4	88.0 <sup>b</sup>	44.5	219.2 <sup>b</sup>
Number of wet days	1900	mean [days/year]	162.9	135.5	98.3	166.7	116.4	152.3	117.4	135.9	137.2
		rel	7.6 <sup>a</sup>	7.2	-	12.2 <sup>b</sup>	13.4 <sup>b</sup>	10.7 <sup>b</sup>	18.5 <sup>b</sup>	-	12.9 <sup>b</sup>
		abs	12.6 <sup>a</sup>	9.7	-	20.3 <sup>b</sup>	15.6 <sup>b</sup>	16.3 <sup>b</sup>	21.7 <sup>b</sup>	-	17.7 <sup>b</sup>
	1960	mean [days/year]	167.9	130.6	102.2	177.3	117.1	163.4	115.7	145.3	146.1
		rel	10.9 <sup>a</sup>	10.9 <sup>a</sup>	0.0	6.9	9.8	2.7	8.1 <sup>a</sup>	-2.6	6.6
		abs	18.3 <sup>a</sup>	14.3 <sup>a</sup>	0.0	12.2	11.5	4.5	9.4 <sup>a</sup>	-3.8	9.7

Note. Changes are both from the long and short time series; note that the trends starting in 1960 are based on substantially more stations. The changes are multiplied with the length of the period, 120 and 60 years for the time series starting in 1900 and 1960, respectively. rel is the change in relative terms over the period, whereas abs is the trend in absolute measures (units of mm, days, and mm). The no-data is in regions where we find it misleading to calculate the trends because of the poor station coverage.

<sup>a</sup>Significant at the 5% confidence level. <sup>b</sup>Significant at 99% confidence level.

drizzle days. This is in contrast to the hypothesis that a warmer climate dominated by the thermodynamic mechanism would have more days of heavy precipitation and fewer days of drizzle, leading to a general decrease in the number of wet days. Climate models show fewer days of drizzle at the end of the century compared to present over most land areas in a low-emission scenario (Sun et al., 2007), but the result is highly dependent on model resolution (Stephens et al., 2010). In contrast to the trend in the absolute contribution of the precipitation rates to the annual total precipitation, the relative contribution decreases at the lower precipitation rates and increased at higher rates (Figure S2b in Supporting Information S1). The precipitation intensity has increased by almost 10%

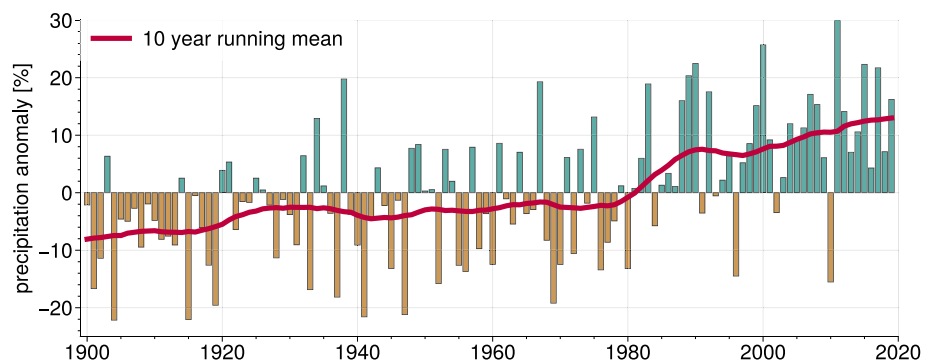


**Figure 3.** Time series of annual mean precipitation anomalies relative to the whole time series. The thin red line indicates number of averaging years is less than the length of the sliding averaging-window.



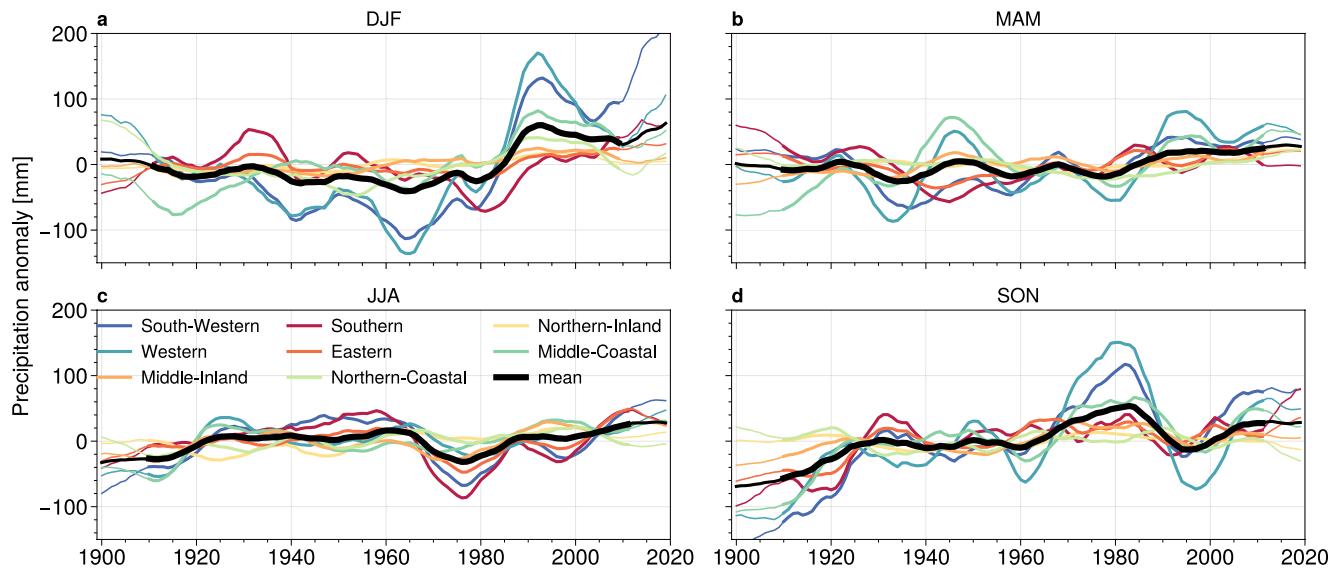


**Figure 4.** Seasonal 10 year running mean precipitation anomalies for each region relative to the whole time series.

in Norway since 1900. The precipitation increase in Norway is due to both increased frequency and intensity. It is neither constrained to the upper percentiles nor is it happening at the expense of the lower percentiles.

### 3.4. Changes in Intense and Extreme Precipitation

To investigate changes in intense and extreme precipitation, we use quantile regression as well as extreme value theory.

The 95th and 99th percentiles show a positive change in 90% of the OP1900-stations using quantile regression, and half of these trends are significant at the 5% significance level. That the absolute increase is becoming larger for the higher percentiles and that most stations exhibit a positive trend is visible in Figure 5 top panel (absolute changes). The relative changes of the 99th percentile are larger than the mean in 49% of the stations in Norway and 69% of the stations for the 95th percentile, consistent with the notion that intense precipitation will increase faster than the mean in the future (Myhre et al., 2019) (Figure 5, second row). Although more stations show negative trends at even higher percentiles (99.5th and 99.9th), the majority still show positive trends (96%/76% OP1900/OP1960), but few of the trends are significant. The 95th percentile increases significantly in South-Western (23%), Northern-Inland (23%), Eastern (16%), and Middle-Coastal (25%). Despite the significant increase of the 95th percentile, the fraction of the 95th percentile to the total annual precipitation has only increased significantly in South-Western (increased by 9% over the past 120 years), Northern-Inland (6.5%), and Middle-Coastal (9.6%). At lower percentiles (25th to 75th), the trends are both positive and negative but small (<1 mm/60 years/<10%).

Calculating the changes in the number of days of intense precipitation based on a constant threshold for the 95th, 99th, 99.5th, and 99.9th percentile, most stations show an increase in the number of days exceeding the thresholds (Figure 5, third panel), although not necessarily significant. Days exceeding the 95th percentile increased by 4.9 days over 120 years (30%), the 99th percentile increased by 0.8 days (24%), while there is no trend for the 99.9th percentile. The relative trend is of similar magnitude for the different percentiles. In Middle-Coastal, the days with precipitation exceeding the 95th percentile have increased by 12 days in the past 120 years, and the trend is steeper in OP1960 (0.7 days/year) than OP1900 (0.04 days/year).

The bottom panel of Figure 5 shows the results from fitting a GEV-distribution to the annual maxima and introducing time as a covariate to the location parameter. Although the uncertainties are large (not shown), most stations have a positive trend in the magnitude of the 100-year events (on average, 40% increase), and the waiting time is reduced by 25 years. However, some of the stations show more than 60 years reduction in waiting time for a 100 year event. It is worth noting that all significant trends are positive (23% of the stations). In addition, the overall pattern is qualitatively consistent with the trends in the quantile regression.

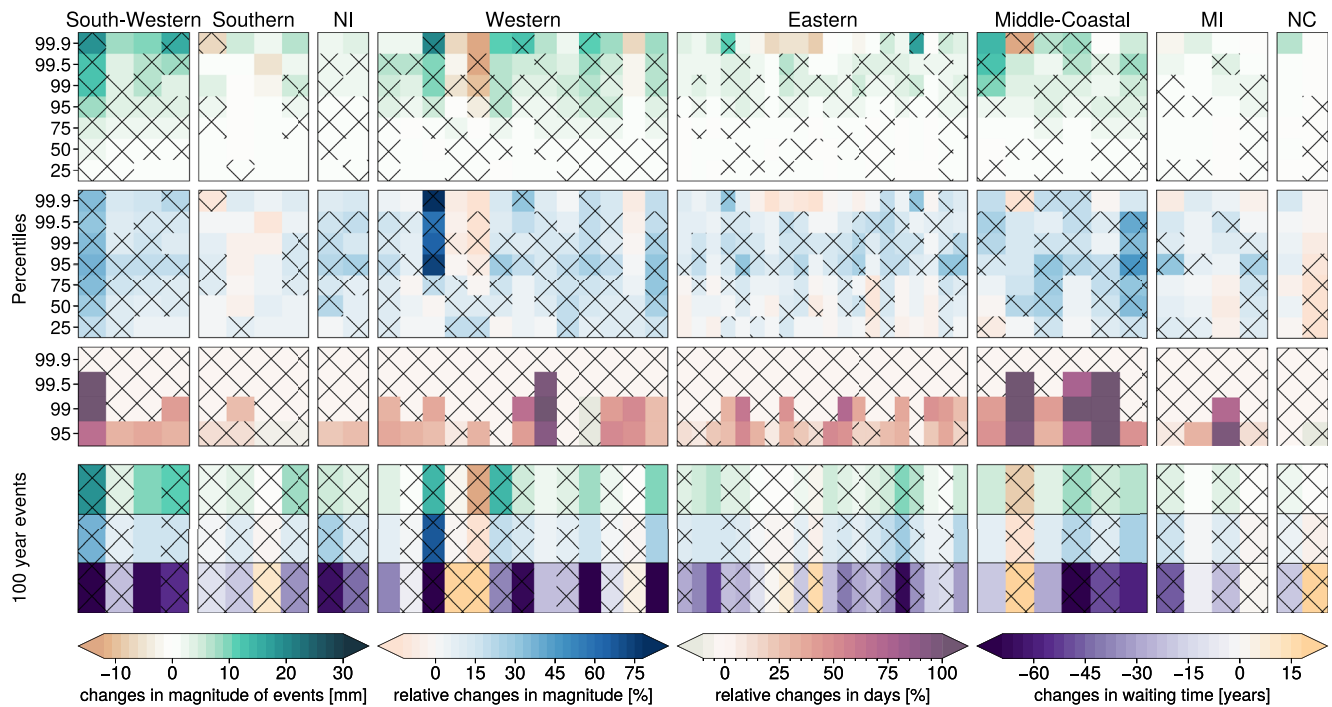


**Figure 5.** Summary of the changes in extreme and intense precipitation. Each tile along the x-axis represents the individual stations grouped together in regions. Top panel: Changes in percentiles grouped by regions for all stations available from 1900 from quantile regression. The upper percentiles (>95) are based on all days, while the lower are based on only the wet days to avoid zero precipitation at the lower percentiles. Second panel: same as top, but for relative changes. Third panel: Trend in relative number of days exceeding a percentile. Bottom panel: Results from the GEV-fitting, split into three rows: (a) changes in the absolute magnitude of 100 year events, (b) changes in the relative magnitude of 100 year events, (c) changes in waiting time in years. Note that the changes are given over a 120 year period (1900–2019). NI is Northern-Inland, MI is Middle-Inland, and NC is Northern-Coastal. Hatching indicates non-significant trends at the 95% significant level.

Some variability in the sign of the trends is expected as all statistical tests are designed to have a specified false discovery rate. Sun et al. (2021) found that for the Rx1day index (the annual maximum precipitation), 10% of the stations in Europe showed significant increasing trends at the 95% confidence interval, which was larger compared to what can be expected by chance alone (between 0% and 6%). Although not directly comparable, 18% of the stations show a significant increasing trend in Norway for the 99th percentile, which on average occur 4 times a year. The 3.6% stations showing significant negative trends are, on the other hand, within the range of what can be considered “due to chance,” and there are no systematic negative trends within or between regions. The overall tendency is thus toward more intense precipitation, although the interannual variability is large. Furthermore, the fact that the two different methods agree corroborates that the extreme precipitation has increased over the past century.

#### 4. Drivers of Annual Precipitation Variability and Trends

What has caused the change in annual mean precipitation? We have described the statistical properties of how the precipitation has changed over the past 120 years. To relate the observed annual mean precipitation increase to either thermodynamic or dynamic changes, we use the diagnostic model outlined in Equation 1. The diagnostic model estimates precipitation – based on pseudoadiabatic ascent – for three different reanalysis products, ERA-20C, 20CRv3, and ERA5. We show the annual relative anomalies of the estimated precipitation (pseudoadiabatic precipitation, [PAP]) compared to the observed precipitation (OP1900) and precipitation from ERA-20C (P\_ERA-20C) and 20CRv3 (P\_20CRv3) in Figure 6. Because observations represent point-processes rather than area averages as models do, we bin the observations on a  $1^\circ \times 1^\circ$  latitude-longitude grid and do the average of all stations in a grid box prior to averaging over all the grid boxes in a region. This way, we avoid emphasizing regions with a high station density but note that we are comparing PAP to a smaller set of grid points which can cause some discrepancies when comparing PAP to OP1900.

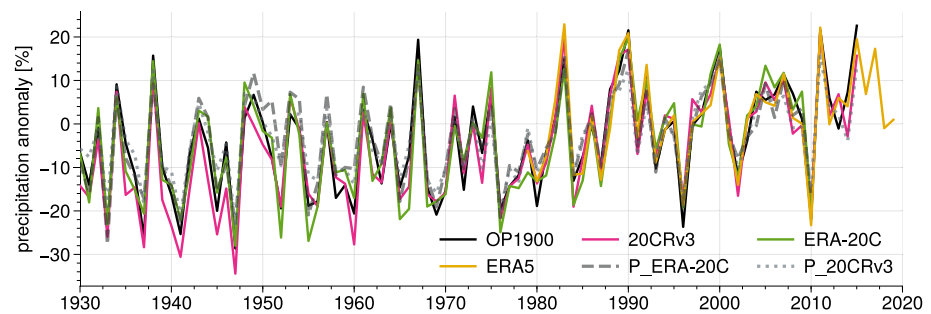


**Figure 6.** Pseudoadiabatic precipitation based on ERA5, ERA-20C, and 20CRv3, observed precipitation (OP1900), and precipitation from reanalysis (P\_ERA-20C and P\_20CRv3) anomalies compared to the 1980–2010 average over Norway.

The number of pressure observations assimilated into the reanalysis in Northern Europe was sparse before 1935 (Slivinski et al., 2019) and the quality of the reanalyses is more questionable before 1950 in terms of circulation indices such as the North Atlantic and Arctic Oscillations (Bloomfield et al., 2018; Poli et al., 2016). However, we find that PAP correlates well with OP1900 after 1930 ( $r > 0.9$ ) in both reanalyses, and considerably higher than between 1900 and 1930 ( $r = 0.68$ ) on an annual time scale. We therefore omit the period 1900–1930 from our analysis.

The absolute level of PAP is underestimated compared to OP1900, and more so using ERA-20C than both 20CRv3 and ERA5 (see a summary of key numbers in Table S1 of Supporting Information S1). The different magnitude of PAP in ERA-20C compared to 20CRv3 can be linked to the critical relative humidity; although the relative humidity is consistently higher in 20CRv3 than in ERA-20C, we have used the same critical relative humidity. However, the variability and the relative anomalies are similar between PAP using all reanalysis products and OP1900, indicating that the relative humidity mainly affects the magnitude of precipitation and not the variability.

In addition to a high temporal correlation on an annual time scale, PAP also shows similar spatial variability characteristics, with higher values in coastal Norway than inland regions. The trend is also relatively well captured in PAP, 20% (17%) in 20CRv3 (ERA-20C) compared to the observed 14%. Note that the trend differs slightly from the result presented earlier (see Table 1) due to a different period (1930–2010) and averaging method. Because the method works adequately, both spatial and temporal, we use Equation 2 to decompose the observed changes in precipitation into contributions from thermodynamics (through changes in temperature and subsequent changes in the water vapor content), dynamics (through changes in vertical velocity), and changes in relative humidity.

Vertical velocity is the key variable in understanding the interannual variability and the long-term trend in annual precipitation (Figure 7).  $P_{\omega^*}$  (precipitation varying only due to the vertical velocity) accounts for 93% (89%) of the yearly variance in PAP based on 20CRv3 (ERA-20C). The contribution from vertical velocity to the precipitation anomalies is mainly negative before 1970 and positive after 1970. This shift coincides with the marked increase in the observed precipitation (Figure 3). In addition, it is worth noting that the absolute magnitude of the vertical velocity differs substantially between ERA-20C and 20CRv3, although the relative anomalies are the same. ERA-20C shows consistently weaker vertical motion than 20CRv3, which provides an additional explanation for why the estimated absolute precipitation values are lower in ERA-20C than 20CRv3.

$P_{\lambda}$  (precipitation varying only due to the relative humidity) accounts for <1% of the interannual variability using 20CRv3 and 45% using ERA-20C. The discrepancy arises because the relative humidity is higher in 20CRv3 than in ERA-20C, but  $RH_c$  is the same. As the relative humidity in 20CRv3 tends to be above  $RH_c$ , the precipitation frequency is mainly decided by the frequency of upward motion, while it is also limited by relative humidity in ERA-20C. Therefore, the correlation of PAP to  $P_{\omega^*}$  in 20CRv3 is higher than in ERA-20C, while  $P_{\lambda}$  accounts for more of the variability in ERA-20C. Lastly,  $P_{T^*}$  (precipitation varying only due to surface temperature) accounts for 58% (61%) in 20CRv3 (ERA-20C). Note that the sum of the variability exceeds 100% because the terms are not independent.

We can decompose the trend into the trends in individual additive terms (Equation 2). The sum of the trends of the individual terms ( $P_{\lambda}$ ,  $P_{\omega^*}$ ,  $P_{T^*}$ ) roughly equals the full estimated PAP trend (the difference is less than 2%

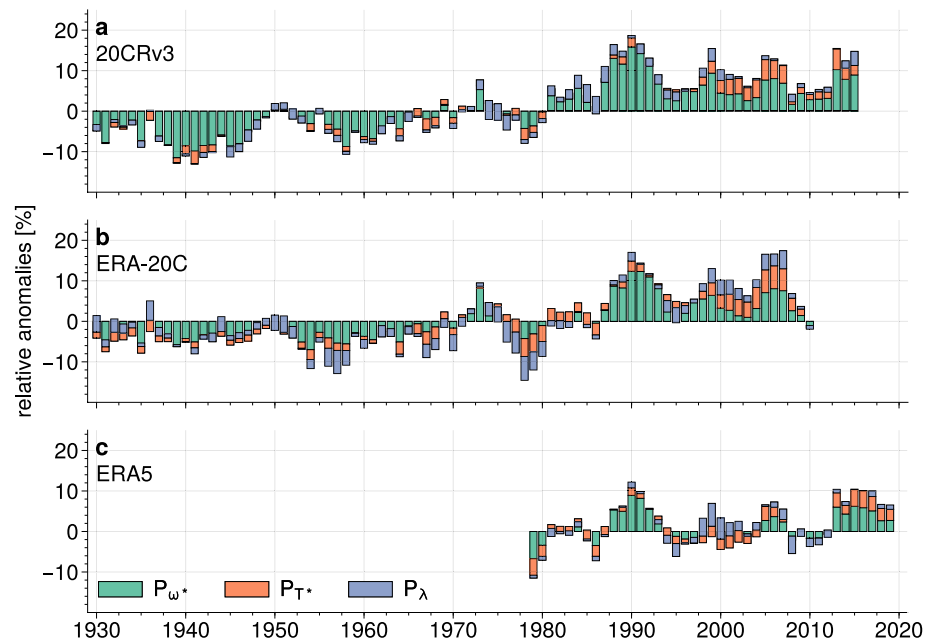


**Figure 7.** 5 year running mean of relative anomalies over Norway.  $P_{\omega^*}$  - contribution from vertical velocity,  $P_{\lambda}$  - relative humidity,  $P_{T^*}$  - temperature. Note that 20CRv3 (a) and ERA-20C (b) use the same averaging period (1930–2010), whereas ERA5 (c) use the whole period available as the reference (1979–2019).

using both 20CRv3 and ERA-20C). However, the relative trends in PAP are overestimated compared to OP1900's in 20CRv3 (5% higher using 20CRv3). Decomposing the trends yield no contribution from  $P_{\lambda}$  in ERA-20C nor 20CRv3 between 1930 and 2010 because there is no trend in relative humidity over Norway. Changes in  $P_{\omega^*}$  accounts for 86% of the total trend in ERA-20C, and 84% in 20CRv3, while  $P_{T^*}$  comprises the rest. In ERA5, between 1979 and 2019, the slightly positive trend in  $P_{\omega^*}$  is directly offset by the negative trend in  $P_{\lambda}$ , while  $P_{T^*}$  accounts for 93% of the trend. Consistent with ERA5, the trend is smaller in  $P_{\omega^*}$  in ERA-20C and 20CRv3 between 1979 and 2019.

To estimate the sensitivity of the surface temperature to precipitation, we do a linear regression of PAP to the near-surface temperature over Norway in the respective reanalysis. The temperature increase in ERA-20C is only 0.6 K over Norway, while it is 0.7 K in 20CRv3, less than the observed 1K increase (Hanssen-Bauer et al., 2017). For 20CRv3 (ERA-20C), this yields a sensitivity to temperature of 10%/K (12%/K) of PAP to temperature, and 4.5%K (5%/K) for  $P_{T^*}$  in 20CRv3 (ERA-20C). The sensitivity of  $P_{T^*}$  to temperature is slightly less than we would expect from pseudoadiabatic scaling.  $P_{\omega^*}$  sensitivity to temperature is 8%/K in 20CRv3 and 6.8%/K in ERA-20C. The main discrepancy between the reanalyzes is in  $P_{\lambda}$ , which shows no relation to temperature in 20CRv3, while it is positive (6.8%/K) in ERA-20C. However, this difference is most likely due to the discrepancies in RH and  $RH_c$ , as discussed earlier.

The sensitivity of the dynamic contribution to temperature is what differs most compared to Pfahl et al. (2017), who showed a sensitivity in the dynamic contribution in the future of 1%–3%/K over Scandinavia. However, the sensitivity in Pfahl et al. (2017) is calculated based on the model ensemble mean, and individual members' dynamic components may be more sensitive to changes in temperature. This is reflected in the large uncertainty in the future changes in the dynamic component (Pfahl et al., 2017). In addition, part of the discrepancy may be because we regress the dynamic component against changes in annual mean temperature in Norway rather than the global mean temperature. Furthermore, we have calculated the dynamic component directly, and taken the seasonality into account of the decomposition, which differs from the method of Pfahl et al. (2017).

Although the vertical velocity is argued to change little in the future, we find that the vertical velocity in the reanalyzes has changed over the past century. Vertical velocity is thought to change little with climate change in the extratropics because it does not depend on either static stability or latent heating in a non-convective environment (O'Gorman, 2015). However, in ETCs, the asymmetry of vertical velocity and hence the strength of the

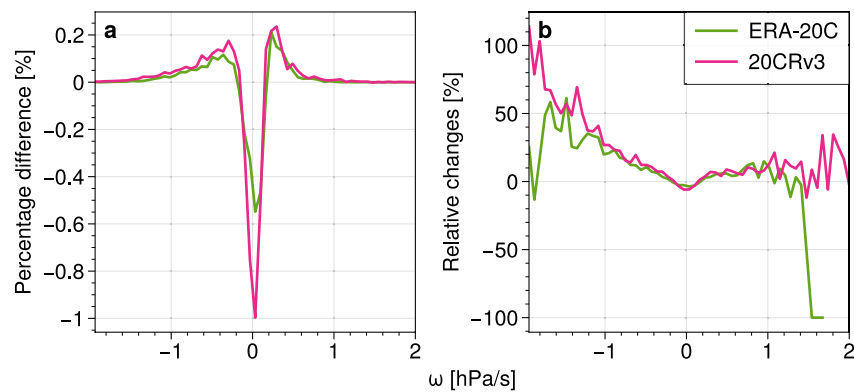


**Figure 8.** Changes in the distribution of  $\omega$  at 850 hPa, calculated as the change of the number of occurrences in each intensity of the vertical velocity between 1970 and 2010 compared to 1930–1970. (a) The change in the probability for the different intensities of vertical velocity. (b) Same as a, but normalized by the probability of an intensity to occur in the former period.

upward motion has the potential to increase in the future because of increased latent heating (Tamarin-Brodsky & Hadas, 2019). If the asymmetry of the vertical motion increases, this may not be visible in the average changes of the vertical velocity but might be vital for precipitation changes as its distribution is known to link intimately to the precipitation distribution. Pendergrass and Gerber (2016) found that changing the skewness of the vertical velocity distribution was crucial to represent important characteristics of the changes in precipitation, that is, that extreme precipitation is increasing more than the mean. We, therefore, compare how the mean distribution of  $\omega$  has changed over Norway between 1970–2010 and 1930–1970 (Figure 8). For all pressure levels (Figure 8a, only 850 hPa shown), there are fewer occurrences of weak vertical motion in the later period than in the earlier period, indicating that the width of the distribution increased. Both the upward and downward intensity increase in both reanalysis products, but the change is more pronounced in 20CRv3 than ERA-20C. Although the overall change is small (2% more days of upward motion in the later period compared to the earlier period), some bins show substantial changes (Figure 8b). The strongest upward motion increases with more than 50% in ERA-20C and more than 100% in 20CRv3. The changes in vertical velocity distribution reveal that the tail is longer for changes in upward motions ( $\omega < 0$ ) than downward motions, which agrees qualitatively with the observed asymmetric precipitation response. In addition, the frequency of days with upward motion is increasing, consistent with the observed frequency increase. However, the relative increase in the occurrences of upward motion is considerably smaller than the observed frequency increase.

#### 4.1. Precipitation Increase From 1980 to 2010

Notably, almost half of the precipitation increase occurred between 1980 and 1990 (Figure 3). We focus on this period to better understand what caused this increase. The model captures the increase and the dry years before the increase (Figure 6). While anomalous low relative humidity and temperatures cause the dry years (negative contributions from  $P_\lambda$  and  $P_{T^*}$ ), enhanced vertical velocity (positive contribution from  $P_{\omega^*}$ ) cause the wet period (Figure 7). The positive contribution from vertical velocity is consistent across all reanalysis products, although the magnitude differs.

ETCs are linked to precipitation as they constitute areas of large-scale ascent and subsequent condensation and precipitation. In addition, ETCs are associated with fronts and often intense moisture transport, which, as it approaches Norway, is forced over topography and causes heavy precipitation. Hawcroft et al. (2012) found that >75% of all winter precipitation over Norway can be associated with ETCs. The storm track activity has been analyzed in previous studies using different reanalyses and proxies. Feser et al. (2015); Chang and Fu (2003) found that storm track activity was weakest during the 1960s and increased until the 1990s before it decreased back to average values until 2010. The increase in storm track activity was particularly prominent over the Eastern Atlantic and Europe (Chang & Fu, 2003). The timing of the lowest storm track activity fits well with the all-time driest winter in coastal regions in DJF in the 1960s and the subsequent increase in precipitation to an all-time maximum in DJF in the 1990s (Figure 4a). The decrease in storm track activity coincides with the decline

in the importance of vertical velocity in our diagnostic model (Figure 7), and we, therefore, hypothesize that the changes in the vertical velocity and hence the dynamic component of precipitation are associated with the storm track variability in the North Atlantic. In addition, as mentioned before, the asymmetry of vertical velocity in ETCs can increase because of increased latent heating due to increasing temperatures (Tamarin-Brodsky & Hadas, 2019). After 2000, the contribution from  $P_r^*$  and  $P_\lambda$  dominates, particularly in ERA-20C, simultaneously as coastal DJF precipitation decreases. The increase after 2000 is happening in all regions and all seasons. We note that this is consistent with a pure thermodynamic response in precipitation to the increasing temperatures in Norway after 2000. Furthermore, dynamic or circulation changes over Europe are consistent with other studies. Sippel et al. (2020) linked the rapid temperature increase in the 1980s over Europe to circulation changes. Furthermore, van Haren et al. (2013) found that errors in the climate model simulated circulation patterns were the main reason for the bias in precipitation trends over Northern Europe, rather than a direct effect of the models' coarse resolution on precipitation. However, making an exact link of ETCs to precipitation changes in Norway and changes in vertical velocity requires further research and is beyond the scope of this paper. In addition, previous studies have determined that the dynamic component has been crucial for changes in extremes. Ali and Mishra (2018) found that the dynamic component scaled with more than 10%/K for extreme precipitation events over India and was substantially larger than the thermodynamic scaling. When decomposing the moisture budget for a record-breaking wet January in Britain, Oueslati et al. (2019) found the dynamic component to play the most important role. We show that the dynamic component is also the main factor deciding the interannual variability in mean precipitation over long timescales in Norway.

#### 4.2. Applicability of Method

Although we have only used this method in Norway, we believe we can say something about the general applicability of the method by investigating the method's performance in the different regions. In the individual regions, the correlation between OP1900 (observed precipitation) and PAP (pseudoadiabatic ascent estimated precipitation) drops to a mean of 0.78 in 20CRv3 (min = 0.54, max = 0.88) and 0.68 in ERA-20C (min = 0.4, max = 0.86), and the best agreement is in South-Western and Western, followed by the rest of the coastal regions.

In the inland regions (Eastern, Northern-Inland, and Middle-Inland), PAP is underestimated in summer and overestimated in winter compared to observations and reanalysis-precipitation. Although OP1900 increases from spring to summer in Northern-Inland and Middle-Inland, PAP overestimates the precipitation in SON and DJF. PAP underestimates precipitation in summer in Western and Middle-Coastal, but only compared to reanalyzes-precipitation, not OP1900. However, as the observations are averaged over a smaller number of grid points, it may be that the observations are located where summer precipitation is lower than the regional average or that the summer precipitation is not accurately represented in the reanalyzes. Although ERA5 has a higher resolution and should thus better represent the vertical velocity associated with convection and possibly better capture the seasonal cycle, PAP does not have a better seasonal cycle in ERA5 than the other reanalyzes. This is most likely related to the simplistic nature of the PAP model. An essential assumption of the model is that the moisture supply is unlimited when precipitation occurs, which is not necessarily valid in the inland regions. This may partly account for the overestimation of PAP compared to OP1900, particularly because the method assumes it precipitates for 24 hr. The assumption that precipitation does not evaporate on the way down may lead to an overestimation during drizzle events but is probably less important than the aforementioned simplification. Lastly, ERA-20C and 20CRv3 most likely represent the vertical velocity more accurately in regions where it is governed by synoptic-scale dynamics. The combination of this and the coastal regions having no shortage of moisture supply may explain why the seasonal cycle is better represented in coastal regions where most precipitation falls during SON and DJF.

To conclude, care should be taken in regions where most precipitation falls during strong convective events and regions where the moisture supply is limited if this method is further used for mean precipitation.

#### 5. Uncertainties Associated With Precipitation Measurements

Precipitation measurements are susceptible to a change in location, measurement technique, or installation of windshields. Hanssen-Bauer and Førland (1994) found that the relocation of weather stations accounted for 47% of the detected inhomogeneities in precipitation stations in Norway. Relocation of weather stations can cause

artificially induced trends either because the sheltering conditions are different or because the annual precipitation is different. We might have induced artificially induced trends when we merged stations; however, we discarded the entire station if any breakpoint was detected close to a station merging.

In addition to relocation, wind affects the precipitation catch. Hanssen-Bauer and Førland (1994) found that the installation of windshields was responsible for 30% of the inhomogeneities in the long precipitation series in Norway. The installation of windshields improves the catch, particularly in regions where a large portion of the precipitation falls as snow, but does not substantially increase the catch, even in windy conditions, for temperatures  $<3^{\circ}\text{C}$  (Wolff et al., 2015). In regions and mountainous areas where most precipitation falls as snow, a transition from snow to rain can also induce trends in measured precipitation. Such a trend would be mainly visible in the onset or offset of winter. However, it is impossible to determine whether the observed trends are due to a snow-rain transition. We, therefore, took the conservative approach and threw out all stations with significant breakpoints detected by the homogeneity test. The installation of windshields and snow-rain transition is likely why so few stations at high elevations and in Northern Norway passed the quality control.

In contrast, winters in South-Western and Western tend to be mild and rainy, and the installation of windshields is thought to be of minor importance (Hanssen-Bauer & Førland, 1994), as well as the snow-rain transition. Furthermore, 70% of all windshield installations were done in the period 1906–1910 (Hanssen-Bauer & Førland, 1994), and we find that the trend from 1930 to 2010 is not substantially different from the trend from 1900 to 2019. It is worth noting that, overall, the trends from the reanalyzes precipitation match the observed and the estimated precipitation (PAP).

Except for automatization gradually happening over the last decade, the sampling routine and bucket diameter have not changed. Automatization was responsible for 12% of the detected breakpoints between 1960 and 2018 and generally reduced the precipitation catch (Kuya & Tveito, 2021). At the same time, the sampling frequency has increased in some stations from one to three times a day, which might influence the very low precipitation amounts due to decreased evaporation.

Our calculated trends are consistent with previous studies (Hanssen-Bauer, 2005; Hanssen-Bauer et al., 2017; Hanssen-Bauer & Førland, 1998, 2000). Despite the uncertainties related to precipitation measurements, we are confident that the trends presented here represent the actual trends except in the Northernmost regions where the station coverage remains poor. Lastly, our study shows that 20th-century reanalyzes are not only providing accurate estimates of precipitation in Europe (Poli et al., 2016) but can also be representative for smaller areas such as Norway.

## 6. Conclusions

We have analyzed observations of daily accumulated precipitation from a network of stations that measured continuously between 1900 and 2019 and introduced and used a diagnostic model to assess the mechanisms responsible for the historical precipitation variation in Norway. We find that in Norway:

1. Precipitation has increased by 19% between 1900 and 2019. Notably, almost half of the increase occurred between 1980 and 1990 in winter. In contrast, the precipitation increase after 2000 occurs in all seasons.
2. Both frequency and intensity contribute to the precipitation increase. Although we find a positive trend across all precipitation rates, intense precipitation's absolute magnitudes increase faster than the mean.
3. The long-term trend and year-to-year variation in precipitation can be approximated with pseudoadiabatic ascent and hence three parameters: vertical velocity, temperature, and relative humidity. Changes in precipitation can then be related to these three parameters.
4. Vertical velocity is the key variable for precipitation variability and the long-term trend.
5. The precipitation increase between 1980 and 1990 appears dramatic, but this is partly because the late '60s and '70s were anomalously dry. While low temperatures and relative humidity can explain some of the period's dryness, anomalous upward motion, and thus the dynamic contribution, dominates the wet period in the late '80s and early '90s, which corresponds to a time period where previous studies have found increased storm track activity in the North-Eastern Atlantic.

6. From 2000 and onward, the vertical velocity is less important than before. Instead, the high precipitation amounts link to anomalously high temperatures and relative humidity, and, consistent with a pure thermodynamic response, the precipitation increase is happening in all regions and seasons.

The precipitation increase in Norway is larger than what can be explained by increased water vapor in the atmosphere alone. Our decomposition of the precipitation increase points to the importance of vertical velocity, both for the variability and long-term trend. The dynamic part is the most uncertain parameter regarding precipitation changes in climate models. Hence, to predict precipitation changes in the future, it is critical to understand the mechanisms responsible for the changes in vertical motion in the past and the weather that governs it.

### Data Availability Statement

The precipitation station data from the Norwegian Meteorological Institute used in this study is accessible at <https://frost.met.no/>. ERA5 was downloaded from the Copernicus Climate Change Service (C3S) Climate Data Store (<https://cds.climate.copernicus.eu/cdsapp>), and ERA-20C from ECMWF (<https://apps.ecmwf.int/datasets/data/era20c-daily>). NOAA/CIRES/DOE 20th Century Reanalysis V3 (20CRv3) data was provided by the NOAA PSL, Boulder, Colorado, USA, from their website at [https://psl.noaa.gov/data/gridded/data.20thC\\_ReanV3.html](https://psl.noaa.gov/data/gridded/data.20thC_ReanV3.html). The software for the penalized maximum  $F$ -test used for homogeneity testing of the stations is available for download at <http://etcccdi.pacificclimate.org/software>. We used the extRemes package (Gilleland & Katz, 2016) for extreme value analysis, available for download at <https://CRAN.R-project.org/package=extRemes>.

### Acknowledgments

We thank the Norwegian Meteorological Institute for making the precipitation station data freely accessible at [frost.met.no](https://frost.met.no). ERA5 was downloaded from the Copernicus Climate Change Service (C3S) Climate Data Store. The authors thank ECMWF for providing ERA-20C reanalysis data. Support for the Twentieth Century Reanalysis Project data set is provided by the US Department of Energy, Office of Science Innovative and Novel Computational Impact on Theory and Experiment program, and Office of Biological and Environmental Research, and by the National Oceanic and Atmospheric Administration Climate Program Office. We would also like to thank three anonymous reviewers for their constructive comments on this manuscript. This research was supported by the Geophysical Institute, University of Bergen, and the Bjerknes Centre for Climate Research, University of Bergen.

### References

- Alexander, L. V., Zhang, X., Peterson, T. C., Caesar, J., Gleason, B., Klein Tank, A. M., et al. (2006). Global observed changes in daily climate extremes of temperature and precipitation. *Journal of Geophysical Research*, *111*, D05109. <https://doi.org/10.1029/2005JD006290>
- Ali, H., & Mishra, V. (2018). Contributions of dynamic and thermodynamic scaling in subdaily precipitation extremes in India. *Geophysical Research Letters*, *45*(5), 2352–2361. <https://doi.org/10.1002/2018GL077065>
- Azad, R., & Sorteberg, A. (2017). Extreme daily precipitation in coastal western Norway and the link to atmospheric rivers. *Journal of Geophysical Research: Atmospheres*, *122*, 2080–2095. <https://doi.org/10.1002/2016JD025615>
- Benedict, I., Ødemark, K., Nipen, T., & Moore, R. (2019). Large-scale flow patterns associated with extreme precipitation and atmospheric rivers over Norway. *Monthly Weather Review*, *147*(4), 1415–1428. <https://doi.org/10.1175/MWR-D-18-0362.1>
- Bloomfield, H. C., Shaffrey, L. C., Hodges, K. I., & Vidale, P. L. (2018). A critical assessment of the long-term changes in the wintertime surface Arctic Oscillation and Northern Hemisphere storminess in the ERA20C reanalysis. *Environmental Research Letters*, *13*(9), 094004. <https://doi.org/10.1088/1748-9326/aad5c5>
- Bohlinger, P., & Sorteberg, A. (2018). A comprehensive view on trends in extreme precipitation in Nepal and their spatial distribution. *International Journal of Climatology*, *38*(4), 1833–1845. <https://doi.org/10.1002/joc.5299>
- Chang, E. K., & Fu, Y. (2003). Using mean flow change as a proxy to infer interdecadal storm track variability. *Journal of Climate*, *16*(13), 2178–2196. <https://doi.org/10.1175/2773.1>
- Clausius, R. (1850). Ueber die bewegende Kraft der Wärme und die Gesetze, welche sich daraus für die Wärmelehre selbst ableiten lassen. *Annalen der Physik*, *155*(3), 368–397. <https://doi.org/10.1002/andp.18501550306>
- Collier, C. G. (1975). A representation of the effects of topography on surface rainfall within moving baroclinic disturbances. *Quarterly Journal of the Royal Meteorological Society*, *101*(429), 407–422. <https://doi.org/10.1002/qj.49710142902>
- Cram, T. A., Compo, G. P., Yin, X., Allan, R. J., McColl, C., Vose, R. S., et al. (2015). The international surface pressure databank version 2. *Geoscience Data Journal*, *2*(1), 31–46. <https://doi.org/10.1002/GDJ3.25>
- Fan, L., & Chen, D. (2016). Trends in extreme precipitation indices across China detected using quantile regression. *Atmospheric Science Letters*, *17*(7), 400–406. <https://doi.org/10.1002/asl.671>
- Feser, F., Barcikowska, M., Krueger, O., Schenk, F., Weisse, R., & Xia, L. (2015). Storminess over the North Atlantic and northwestern Europe—A review. *Quarterly Journal of the Royal Meteorological Society*, *141*(687), 350–382. <https://doi.org/10.1002/qj.2364>
- Gilleland, E., & Katz, R. W. (2016). ExtRemes 2.0: An extreme value analysis package in R. *Journal of Statistical Software*, *72*(8). <https://doi.org/10.18637/jss.v072.i08>
- Haltiner, G. J., & Williams, R. T. (1980). *Numerical prediction and dynamic meteorology* (2nd ed.). Wiley and Sons.
- Hanssen-Bauer, I. (2005). *Regional temperature and precipitation series for Norway: Analyses of time-series updated to 2004* (Tech. Rep. No. 15). Norwegian Meteorological Institute.
- Hanssen-Bauer, I., & Førland, E. (1998). *Annual and seasonal precipitation variations in Norway 1896-1997* (Tech. Rep.). Norwegian Meteorological Institute.
- Hanssen-Bauer, I., & Førland, E. (2000). Temperature and precipitation variations in Norway 1900-1994 and their links to atmospheric circulation. *International Journal of Climatology*, *20*(14), 1693–1708. [https://doi.org/10.1002/1097-0088\(20001130\)20:14<1693::aid-joc567>3.0.co;2-7](https://doi.org/10.1002/1097-0088(20001130)20:14<1693::aid-joc567>3.0.co;2-7)
- Hanssen-Bauer, I., & Førland, E. J. (1994). Homogenizing long Norwegian precipitation series. *Journal of Climate*, *7*(6), 1001–1013. [https://doi.org/10.1175/1520-0442\(1994\)007<1001:hlnps>2.0.co;2](https://doi.org/10.1175/1520-0442(1994)007<1001:hlnps>2.0.co;2)
- Hanssen-Bauer, I., Førland, E. J., Haddeland, I., Hisdal, H., Lawrence, D., Mayer, S., et al. (2017). Climate in Norway 2100. NCCS report no. 1/2017 (pp. 1–47). Retrieved from [www.miljodirektoratet.no/M741](http://www.miljodirektoratet.no/M741)
- Hanssen-Bauer, I., Tveit, O. E., & Szewczyk-Bartnicka, H. (2006). *Comparison of grid-based and station-based regional temperature and precipitation series* (Tech. Rep. No. 04). Norwegian Meteorological Institute.



- Hawcroft, M. K., Shaffrey, L. C., Hodges, K. I., & Dacre, H. F. (2012). How much Northern Hemisphere precipitation is associated with extratropical cyclones? *Geophysical Research Letters*, *39*(24), 2012GL053866. <https://doi.org/10.1029/2012gl053866>
- Haylock, M. R., Hofstra, N., Klein Tank, A. M., Klok, E. J., Jones, P. D., & New, M. (2008). A European daily high-resolution gridded data set of surface temperature and precipitation for 1950–2006. *Journal of Geophysical Research*, *113*, D20119. <https://doi.org/10.1029/2008JD010201>
- Heikkilä, U., & Sorteberg, A. (2012). Characteristics of autumn–winter extreme precipitation on the Norwegian west coast identified by cluster analysis. *Climate Dynamics*, *39*(3), 929–939. <https://doi.org/10.1007/s00382-011-1277-9>
- Hersbach, H., Bell, B., Berrisford, P., Hirahara, S., Horányi, A., Muñoz-Sabater, J., et al. (2020). The ERA5 global reanalysis. *Quarterly Journal of the Royal Meteorological Society*, *146*(730), 1999–2049. <https://doi.org/10.1002/qj.3803>
- Hu, L., Nikolopoulos, E. I., Marra, F., & Anagnostou, E. N. (2020). Sensitivity of flood frequency analysis to data record, statistical model, and parameter estimation methods: An evaluation over the contiguous United States. *Journal of Flood Risk Management*, *13*(1), 1–13. <https://doi.org/10.1111/jfr3.12580>
- Kharin, V. V., Zwiers, F. W., Zhang, X., & Hegerl, G. C. (2007). Changes in temperature and precipitation extremes in the IPCC ensemble of global coupled model simulations. *Journal of Climate*, *20*(8), 1419–1444. <https://doi.org/10.1175/jcli4066.1>
- Koenker, R., & Hallock, K. F. (2001). Quantile regression. *The Journal of Economic Perspectives*, *15*(4), 143–156. <https://doi.org/10.1257/jep.15.4.143>
- Kunz, M., & Kottmeier, C. (2006). Orographic enhancement of precipitation over low mountain ranges. Part II: Simulations of heavy precipitation events over southwest Germany. *Journal of Applied Meteorology and Climatology*, *45*(8), 1041–1055. <https://doi.org/10.1175/JAM2390.1>
- Kuya, E. K., & Tveito, O. E. (2021). Homogenization of Norwegian monthly precipitation series for the period 1961–2018 METreport (Tech. Rep. No. 4). Retrieved from [https://www.met.no/publikasjoner/met-report/\\_attachment/download/829d6a8e-1ec8-417d-8231-0268bddac4b-7eb30ca105a6cfd470453976bb8d729a64b25a4/METreport04-21-Homogenizationofprecipitation1961-2018.pdf](https://www.met.no/publikasjoner/met-report/_attachment/download/829d6a8e-1ec8-417d-8231-0268bddac4b-7eb30ca105a6cfd470453976bb8d729a64b25a4/METreport04-21-Homogenizationofprecipitation1961-2018.pdf)
- Mann, H. B. (1945). Nonparametric tests against trend. *Econometrica*, *13*(3), 245–259. <https://doi.org/10.2307/1907187>
- Michel, C., Sorteberg, A., Eckhardt, S., Weijenborg, C., Stohl, A., & Cassiani, M. (2021). Characterization of the atmospheric environment during extreme precipitation events associated with atmospheric rivers in Norway – seasonal and regional aspects. *Weather and Climate Extremes*, *34*, 100370. <https://doi.org/10.1016/j.wace.2021.100370>
- Myhre, G., Alterskjær, K., Stjern, C. W., Hodnebrog, Marelle, L., Samset, B. H., & Stohl, A. (2019). Frequency of extreme precipitation increases extensively with event rareness under global warming. *Scientific Reports*, *9*(1), 2–11. <https://doi.org/10.1038/s41598-019-52277-4>
- O’Gorman, P. A. (2015). Precipitation extremes under climate change. *Current Climate Change Reports*, *1*(2), 49–59. <https://doi.org/10.1007/s40641-015-0009-3>
- Oueslati, B., Yiou, P., & Jézéquel, A. (2019). Revisiting the dynamic and thermodynamic processes driving the record-breaking January 2014 precipitation in the southern UK. *Scientific Reports*, *9*(1), 1–7. <https://doi.org/10.1038/s41598-019-39306-y>
- Pendergrass, A. G., & Gerber, E. P. (2016). The rain is askew: Two idealized models relating vertical velocity and precipitation distributions in a warming world. *Journal of Climate*, *29*(18), 6445–6462. <https://doi.org/10.1175/JCLI-D-16-0097.1>
- Pfahl, S., O’Gorman, P. A., Fischer, E. M., O’Gorman, P. A., & Fischer, E. M. (2017). Understanding the regional pattern of projected future changes in extreme precipitation. *Nature Climate Change*, *7*(6), 423–427. <https://doi.org/10.1038/nclimate3287>
- Poli, P., Hersbach, H., Dee, D. P., Berrisford, P., Simmons, A. J., Vitart, F., et al. (2016). ERA-20C: An atmospheric reanalysis of the twentieth century. *Journal of Climate*, *29*(11), 4083–4097. <https://doi.org/10.1175/JCLI-D-15-0556.1>
- Quaas, J. (2012). Evaluating the “critical relative humidity” as a measure of subgrid-scale variability of humidity in general circulation model cloud cover parameterizations using satellite data. *Journal of Geophysical Research*, *117*, D09208. <https://doi.org/10.1029/2012JD017495>
- Ralph, F. M., Neiman, P. J., & Wick, G. A. (2004). Satellite and CALJET aircraft observations of atmospheric rivers over the Eastern North Pacific Ocean during the winter of 1997/98. *Monthly Weather Review*, *132*(7), 1721–1745. [https://doi.org/10.1175/1520-0493\(2004\)132<1721:sacaoo>2.0.co;2](https://doi.org/10.1175/1520-0493(2004)132<1721:sacaoo>2.0.co;2)
- Sen, P. K. (1968). Estimates of the regression coefficient based on Kendall’s Tau. *Journal of the American Statistical Association*, *63*(324), 1379–1389. <https://doi.org/10.1080/01621459.1968.10480934>
- Seneviratne, S. I., Zhang, X., Adnan, M., Badi, W., Dereczynski, C., Luca, A. D., et al. (2021). Weather and Climate Extreme Events in a Changing Climate. (Eds.). In *Climate change 2021: The physical science basis. contribution of working group I to the sixth assessment report of the intergovernmental panel on climate change (chap. 11)*. Cambridge University Press. Retrieved from [https://www.ipcc.ch/report/ar6/wg1/downloads/report/IPCC\\_AR6\\_WGI\\_Chapter11.pdf](https://www.ipcc.ch/report/ar6/wg1/downloads/report/IPCC_AR6_WGI_Chapter11.pdf)
- Shepherd, T. G. (2014). Atmospheric circulation as a source of uncertainty in climate change projections. *Nature Geoscience*, *7*(10), 703–708. <https://doi.org/10.1038/NGEO2253>
- Sillmann, J., Kharin, V. V., Zwiers, F. W., Zhang, X., & Bronaugh, D. (2013). Climate extremes indices in the CMIP5 multimodel ensemble: Part 2. Future climate projections. *Journal of Geophysical Research: Atmospheres*, *118*, 2473–2493. <https://doi.org/10.1002/jgrd.50188>
- Sinclair, M. R. (1994). A diagnostic model for estimating orographic precipitation. *Journal of Applied Meteorology*, *33*(10), 1163–1175. [https://doi.org/10.1175/1520-0450\(1994\)033<1163:admfeo>2.0.co;2](https://doi.org/10.1175/1520-0450(1994)033<1163:admfeo>2.0.co;2)
- Sippel, S., Fischer, E. M., Scherrer, S. C., Meinshausen, N., & Knutti, R. (2020). Late 1980s abrupt cold season temperature change in Europe consistent with circulation variability and long-term warming. *Environmental Research Letters*, *15*(9), 094056. <https://doi.org/10.1088/1748-9326/ab86f2>
- Slivinski, L. C., Compo, G. P., Whitaker, J. S., Sardeshmukh, P. D., Giese, B. S., McColl, C., et al. (2019). Towards a more reliable historical reanalysis: Improvements for version 3 of the Twentieth Century Reanalysis system. *Quarterly Journal of the Royal Meteorological Society*, *145*(724), 2876–2908. <https://doi.org/10.1002/qj.3598>
- Stephens, G. L., L’Ecuyer, T., Forbes, R., Gettelmen, A., Golaz, J. C., Bodas-Salcedo, A., et al. (2010). Dreary state of precipitation in global models. *Journal of Geophysical Research*, *115*, D24211. <https://doi.org/10.1029/2010JD014532>
- Sun, Q., Zhang, X., Zwiers, F., Westra, S., & Alexander, L. V. (2021). A global, continental, and regional analysis of changes in extreme precipitation. *Journal of Climate*, *34*(1), 243–258. <https://doi.org/10.1175/JCLI-D-19-0892.1>
- Sun, Y., Solomon, S., Dai, A., & Portmann, R. W. (2007). How often will it rain? *Journal of Climate*, *20*(19), 4801–4818. <https://doi.org/10.1175/jcli4263.1>
- Tamarin-Brodsky, T., & Hadas, O. (2019). The asymmetry of vertical velocity in current and future climate. *Geophysical Research Letters*, *46*(1), 374–382. <https://doi.org/10.1029/2018GL080363>
- Tandon, N. F., Zhang, X., & Sobel, A. H. (2018). Understanding the dynamics of future changes in extreme precipitation intensity. *Geophysical Research Letters*, *45*(6), 2870–2878. <https://doi.org/10.1002/2017gl076361>
- Tareghian, R., & Rasmussen, P. (2013). Analysis of Arctic and Antarctic sea ice extent using quantile regression. *International Journal of Climatology*, *33*(5), 1079–1086. <https://doi.org/10.1002/joc.3491>

- Trenberth, K. E., Dai, A., Rasmussen, R. M., & Parsons, D. B. (2003). The changing character of precipitation. *Bulletin of the American Meteorological Society*, 84(9), 1205–1218. <https://doi.org/10.1175/bams-84-9-1205>
- van Haren, R., van Oldenborgh, G. J., Lenderink, G., Collins, M., & Hazeleger, W. (2013). SST and circulation trend biases cause an underestimation of European precipitation trends. *Climate Dynamics*, 40(1–2), 1–20. <https://doi.org/10.1007/s00382-012-1401-5>
- Vicente-Serrano, S. M., García-Herrera, R., Peña-Angulo, D., Tomas-Burguera, M., Domínguez-Castro, F., Noguera, I., et al. (2021). Do CMIP models capture long-term observed annual precipitation trends? *Climate Dynamics*, 58(9–10), 2825–2842. <https://doi.org/10.1007/s00382-021-06034-x>
- Wang, X. L. (2008a). Accounting for autocorrelation in detecting mean shifts in climate data series using the penalized maximal t or F test. *Journal of Applied Meteorology and Climatology*, 47(9), 2423–2444. <https://doi.org/10.1175/2008JAMC1741.1>
- Wang, X. L. (2008b). Penalized maximal F test for detecting undocumented mean shift without trend change. *Journal of Atmospheric and Oceanic Technology*, 25(3), 368–384. <https://doi.org/10.1175/2007JTECHA982.1>
- Westra, S., Alexander, L. V., & Zwiers, F. W. (2013). Global increasing trends in annual maximum daily precipitation. *Journal of Climate*, 26(11), 3904–3918. <https://doi.org/10.1175/JCLI-D-12-00502.1>
- Wolff, M. A., Isaksen, K., Petersen-Øverleir, A., Ødemark, K., Reitan, T., & Brækkan, R. (2015). Derivation of a new continuous adjustment function for correcting wind-induced loss of solid precipitation: Results of a Norwegian field study. *Hydrology and Earth System Sciences*, 19(2), 951–967. <https://doi.org/10.5194/hess-19-951-2015>
- Wu, Y., Wu, S. Y., Wen, J., Xu, M., & Tan, J. (2016). Changing characteristics of precipitation in China during 1960–2012. *International Journal of Climatology*, 36(3), 1387–1402. <https://doi.org/10.1002/joc.4432>